ADVANCED ENGINEERING MATERIALS

COMMUNICATION

DOI: 10.1002/adem.201300061

Realistic Numerical Analysis of a Bioinspired Layered Composite with a Crack: Robust Scaling Laws and Crack Arrest**

By *Yukari Hamamoto* and *Ko Okumura**

Nacre is a prototype of natural strong and tough materials and has been studied extensively. However, no numerical models have been developed that faithfully reflect the layered structure made of alternately stacked soft and hard layers, in order to study the fracture toughness in the presence of a macroscopic crack. In this study, we construct a realistic numerical model by finite element method (FEM) that explicitly takes the layered structure into account and study the stress and deformation fields around a crack. Although we reflect a realistic layered structure, we remarkably find simple scaling laws for the elastic fields, which predict considerable reduction of the stress concentration around the crack tips in exchange for enhancement of the deformation. We also find that the divergence at the crack tips in the scaling law for the stress field is cut-off at the scale of layers, which significantly restrains the maximum stress appearing at the tips. We further find that a crack tip is necessarily stopped at a soft layer and this crack arrest guarantees strong effects of the reduction of the stress concentration and cut-off of the stress singularity. In addition, these toughening mechanisms lead to the prediction of the correct order of the fracture energy experimentally reported in a seminal paper. These mechanisms and the FEM model developed here will be useful for the development of artificial tough advanced materials.

Tough and strong materials in nature quite often exhibit magnificent hierarchical structures. Nacre is probably the most well studied material as such; it is a shining layered composite found inside certain sea shells or on the surface of pearl. This material is remarkable in that only a small amount of the soft component between the layers of the hard component makes the fracture energy a few thousand times as high as that of the monolithic material made of the hard component.[1,2] Accordingly various toughening mechanism of nacre have been proposed,[3–8] and nacre has bioinspired a number of remarkable materials.[9–13] Here, in particular, we focus on a simple model of nacre[14] that provides simple understandings of the type recently revealed for spider webs,[15–17] (although it does not include recently found complex structures beyond the layered structure[18,19]). This is because simple scaling laws were obtained for the model to predict the correct order of the fracture energy of nacre, on the basis of analytical solutions for two crack problems.[14,20]

However, in this model the layered structure is coarse-grained or homogenized: the continuum model is valid on scales larger than the layer period and thus can predict nothing on smaller scales. In particular, this model is insensitive to the position of crack tips, i.e. whether the tips are located in soft or hard layers. To study such issues, we need to construct appropriate numerical models that allow us to seek what happens at scales inaccessible by the coarse-grained continuum model. One such example is a simplified two-dimensional spring-bead model.[21] This model has revealed qualitative features but does not allow quantitative discussions.

In this study, we construct a more realistic numerical model of nacre that explicitly includes the layered structure in the calculation by finite element method (FEM) in the presence of a crack (c.f. ref.[19]). Although we relax some numerically severe conditions in the calculation and explicitly include the layered structure, we find that the scaling laws predicted in the coarse-grained model hold remarkably well at a quantitative level. This suggests robustness of the scaling laws. Furthermore, we find that the scaling laws which hold near the crack tips are cut-off at the length scale of the layered structure. In addition, we find that the stress field near the crack tips significantly changes with the position of the crack tip in the layers, in such a way that a tip of a line crack should be arrested at soft layers. Thereby, we establish, in a clear and robust way at a quantitative level, the following physical principles for the toughening of nacre: reduction of the stress concentration (assisted by enhancement of the deformation), cut-off of the stress singularity, and crack arrest at a soft layer. Furthermore, the FEM model for nacre proposed in this study

[*] *Y. Hamamoto, K. Okumura*
Department of Physics, Graduate School of Humanities and Sciences, Ochanomizu University, 2-1-1, Otsuka, Bunkyo-ku, Tokyo 112-8610, Japan
E-mail: okumura@phys.ocha.ac.jp
Y. Hamamoto
Structural Strength Department, Research Laboratory, IHI Corporation, 1, Shin-nakahara-cho, Yokohama-shi, Kanagawa 235-8501, Japan

[**] *K.O. thanks Professor Takashi Kato (the University of Tokyo) for useful comments. Y.H. thanks Dr. Ohtake, Dr. Nishido and Dr. Tsunori (IHI Corporation) for encouragements. This work is supported by a project, Fusion Materials (Area no. 2206), funded by Grant-in-Aid for Scientific Research on Innovative Areas, from MEXT, Japan.*

ADVANCED ENGINEERING MATERIALS

will provide a solid starting point for investigating the toughening mechanisms of nacre and for predicting mechanical properties of newly designed materials that mimic nacre, at a quantitative level.

1. FEM Model and Simulation Parameters

In this study, we consider a composite composed of thick and hard layers and thin and soft layers. The thicknesses of hard and soft layers are denoted d_h and d_s ($d_h \gg d_s$), respectively, while the elastic moduli are E_h and E_s ($E_h \gg E_s$). We are interested in the small ε limit where the parameter ε, which plays an important role in this study, is defined by

$$\varepsilon = \frac{E_s}{E_h} \cdot \frac{d_h}{d_s}. \quad (1)$$

This parameter is indeed very small:[19,22] in natural nacre, typically, $d_h \simeq d$ and d_s are around 0.5 and 0.025 μm, respectively (the volume of the soft layers are about 5%), while E_s and E_h are of the order of 1 MPa and 100 GPa, respectively, which makes $\varepsilon \simeq 0.0001$.

The FEM analysis was performed for a two-dimensional system under plane strain conditions by using a commercial software, ABAQUS. Thanks to the symmetry, we actually performed a calculation for the region whose area is 1/4 of the actual size. Considering the singular nature of the fields around the crack tips, the mesh size is reduced around the tip as shown in Figure 1a. The total number of the elements is 257 196 for the 1/4 model.

To mimic nacre, we set the basic parameters as $L = 5000 d_s$ and $d_h = 10 d_s$ with $d_s = 10$ nm, where the system size is $2L \times 2L$. We set the elastic moduli of the hard and soft layers to typical values, $E_h = 65$ GPa and $E_s = 1$ MPa, respectively. In this case, $\varepsilon = \varepsilon_0$ with $\varepsilon_0 = 1/6500$. The Poisson's ratios ν of the soft layers and of the hard layers are set to typical values, 0.19 and 0.5, respectively.

To check the ε dependence of the elastic fields around a crack tip, we changed ε by replacing E_s with the other parameters (d_h/d_s, E_h and ν) fixed: we performed calculations also for $E_s = 6.5$ and 65 MPa, namely, for $\varepsilon = 6.5\varepsilon_0 = 1/1000$ and $65\varepsilon_0 = 1/100$. As a reference, we also performed calculations for a monolithic system with a homogeneous Young modulus ($E_h = E_s = 65$ GPa).

We consider below a line crack of length $2a$ is running in the x direction at $y = 0$ in a sample stretched in the y direction. In this case, the direction of the line crack is perpendicular to the layers. We here discuss the perpendicular crack in particular because it is the most important mode of fracture for the shell fish in the shell: cracks created on the surface are always perpendicular to the layers.

We first consider a crack of size $a = 506.5 d_s$ (Throughout this paper, the crack position and size are given by those before the deformation, i.e. before applying the deformation at the edges). In this case, the crack tip is located at a soft layer. We first focus on this case because, in the previous paper,[23] the authors imagined that a tip of a crack perpendicular to layers is stopped at the soft layer. In such a case, the hard layer next to the tip has no macroscopic cracks so that they expected that the stress concentration at the tip tends to be suppressed, which leads to the toughness.

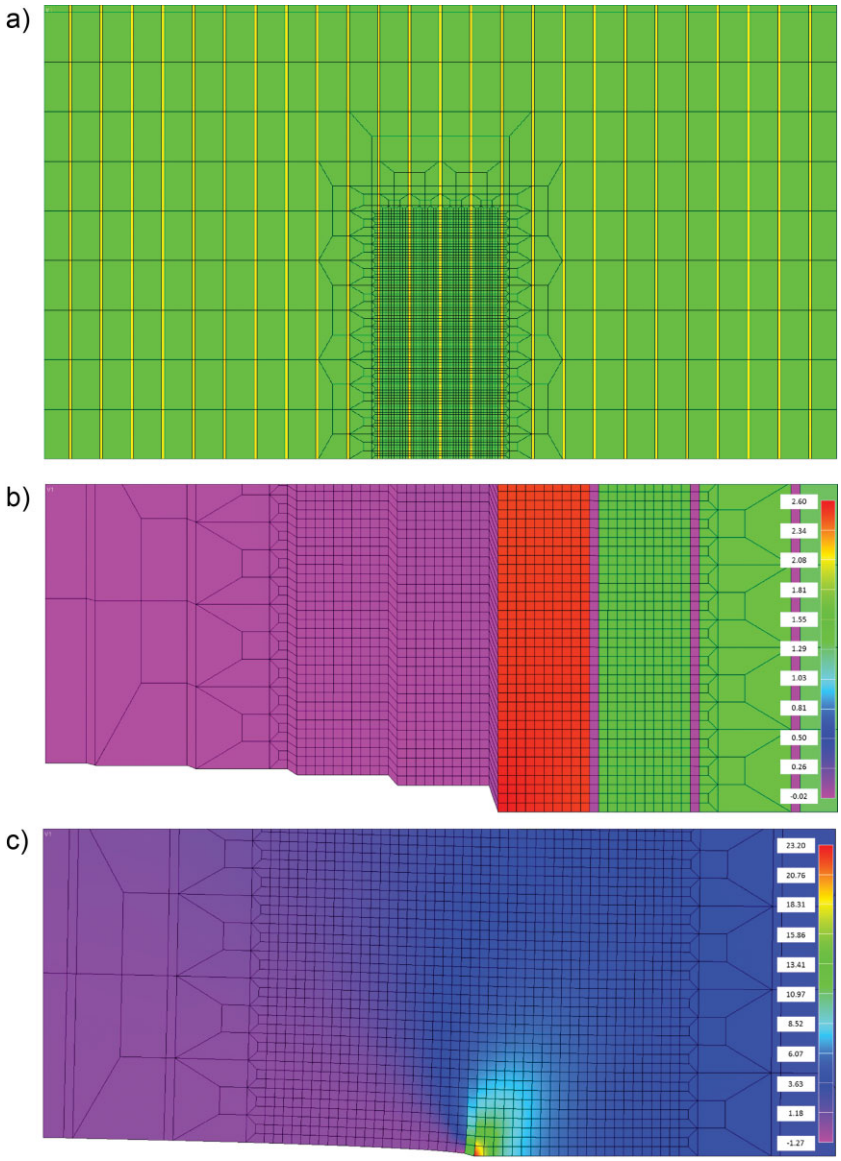

Fig. 1. (a) Mesh for the FEM calculation. Near the crack tip smaller mesh sizes are employed. (b) Contour map of the stress concentration around the crack tip for the nacre model with $\varepsilon = \varepsilon_0$. (c) Contour map for the monolithic model.

2. Results

2.1. Global Stress Distribution and Crack Shape

In Figure 1b and c, the contour maps of the stress distribution around a crack tip together with the crack shapes are given for the nacre model ($\varepsilon = \varepsilon_0$) and, as a reference, for the monolithic system. In the monolithic system, the stress is severely localized and concentrated around the crack tip while the crack takes the standard parabolic shape. On the contrary, in the nacre model the stress is delocalized and only weakly concentrated, thanks to large deformation in the soft layers (the crack takes a zigzag shape), which in turn reduces the deformation of the hard layers (and thus leads to a weak stress concentration). As seen in Figure 1b, when $a = 506.5d_s$ the crack tip is located at a soft layer as mentioned above. In b and c, the same strain is applied but the magnifications in the y direction (to make the deformation more visible) are higher in c than in b: the deformation in the monolithic case is exaggerated five times; Even so, the deformation field at the crack surface is larger in the nacre case.

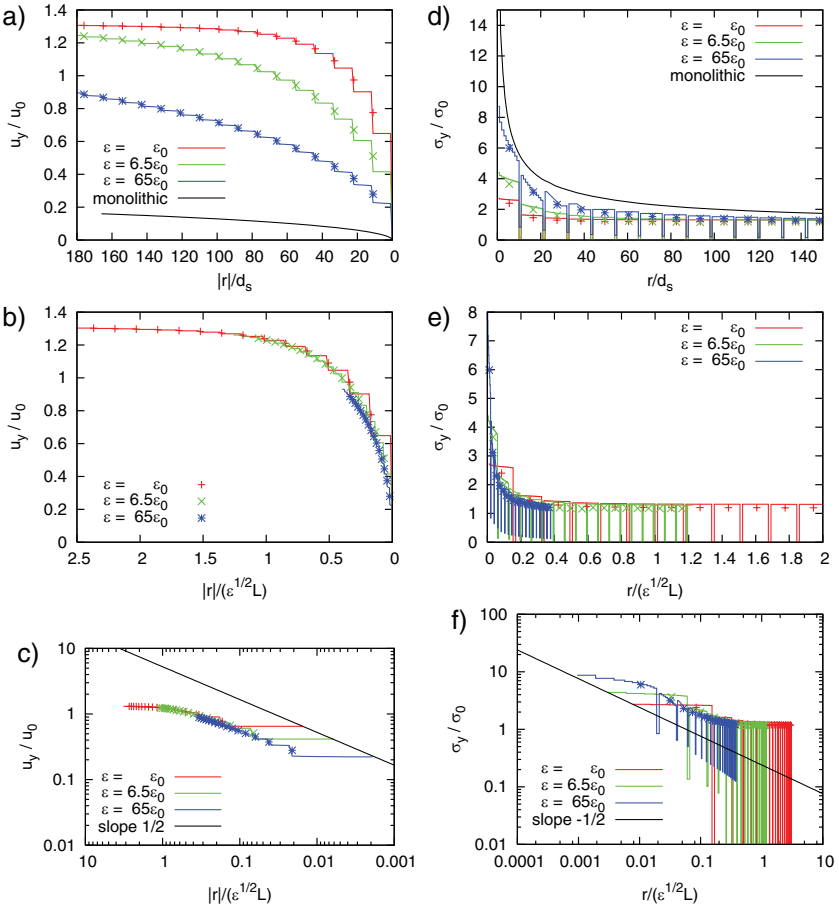

Fig. 2. (a) Comparison of the deformations at the crack surfaces. As predicted by the scaling law, the deformation is augmented, as ε becomes smaller. (b) Collapse of the deformation data by rescaling on the basis of the scaling law. (c) The same plot on log scales. (d) Comparison of the stress fields near the crack tip. As predicted by the scaling law, the stress is reduced, as ε becomes smaller. (e) Collapse of the stress data by rescaling on the basis of the scaling law. (f) The same plot on log scales.

2.2. Deformation and Stress Near a Crack Tip

In Figure 2a and d, the deformation field on the crack surface and the stress field (at $y = 0^+$) are given as a function of the distance r from the right tip of the crack for three values of ε and for the monolithic model. The deformation field is given for the left-hand side of the right crack tip ($r < 0$) while the stress field is given for the right-hand side ($r > 0$): the right tip is placed at the origin of the r-axis, which is parallel to the x-axis. Here and hereafter, the deformation and the stress are renormalized by the values at the edge (remote values u_0 and $E_h u_0/L$, respectively) so that the results are independent of applied strain at the edge (as long as the linear elasticity is valid). As seen in these plots, we see that the curves for the both fields are step-wise (zigzag). Note that in the FEM the stress is constant in each element while the deformation is assigned at each nodal points. In addition, from the plots, we find that the deformation field is enhanced as ε becomes smaller, while the stress field is reduced as ε becomes smaller.

In principle, these behaviors agree with the prediction in the previous studies.[14,20] However, in the previous studies, the elastic fields are coarse-grained or homogenized so that deformation and stress fields as a function of r are given as smooth curves, in contrast with the step-wise (zigzag) curves in the realistic case as demonstrated in Figure 2a and d. In exchange for the unrealistic description on the scale of layer period d, the coarse-grained model allows analytical solutions for crack problems[14,20] because the dominant deformation filed u_y was shown to be governed by an anisotropic Laplace equation (not the biharmonic equation). As a result, the dominant components of deformation and stress (the y and yy components, respectively) are given as a function of the distance r from the right crack tip:

$$\frac{u_y}{u_0} = c_1\sqrt{\frac{|r|}{\varepsilon^{1/2}L}} \tag{2}$$

$$\frac{\sigma_y}{\sigma_0} = c_2\sqrt{\frac{\varepsilon^{1/2}L}{r}} \tag{3}$$

Here, u_0 is the size of a fixed deformation at the top and bottom edges and σ_0 is the corresponding stress ($\sigma_0 = E_h u_0/L$). Under the plane strain conditions, the dimensionless numerical coefficient c_1 and c_2 are given as $2c_3^{-1/4}/\sqrt{\pi}$ and $c_3^{1/4}/\sqrt{\pi}$, respectively, where $c_3 = (1-\nu)/2$. Strictly speaking, in the original model, Poisson's ratios for the soft and hard elements are assumed to be the same. In the present FEM calculation, on the contrary, the Poisson's ratios are 0.19 and 0.5, respectively. Accordingly the factors c_1 and c_2 are 1.41 and 0.450 for the soft

ADVANCED ENGINEERING MATERIALS

elements, while they are 1.596 and 0.399, respectively for the hard elements. Considering the volume fraction of the soft and hard layers, we employ below rough estimates, $c_1 = 1.6$ and $c_2 = 0.4$, for comparison between the theory and the FEM calculation.

We note here that Eqs. (2) and (3) are independent of the crack size (but dependent on L). A similar fact is well-known even for the isotropic case when the size of a crack running in the x-direction is much larger than the sample size in the y-direction; in such a case the elastic fields are governed by the latter (smaller) size. In this anisotropic case, however, the stress and strain distributions around the crack tip are independent of the crack size even if the crack size is comparable to the sample size (this is because the last condition in Eq. (5) can be satisfied even if $a \sim L$ when $\varepsilon \ll 1$). This was first shown in ref.[20] but has not been properly appreciated.

From these scaling laws, the correct order of the fracture energy is predicted in ref.[14]. This was done by assuming the maximum stress σ_M that appears at the crack tip is given by Eq. (3) at $r = d$:[14]

$$\frac{\sigma_M}{\sigma_0} \simeq \sqrt{\frac{\varepsilon^{1/2} L}{d}} \tag{4}$$

Namely, they conjectured that Eq. (3) should be cut-off at the length scale d because below this scale the homogenized view breaks down. This relation is given only at the level of scaling laws: dimensionless numerical coefficients of the order of unity are simply set to one for simplicity. At this level, for example, Young's and shear modulus are not distinguished and Poisson's ratio is suppressed.

Eqs. (2–4) become exact only in the limit specified as

$$d_s \ll d_h \approx d \ll r \ll L, a \text{ and } \varepsilon^{1/2} L \ll a \tag{5}$$

and

$$E_s \ll E_h \text{ such that } \varepsilon = \frac{E_s}{E_h} \cdot \frac{d_h}{d_s} \ll 1 \tag{6}$$

In addition, the sample size in the x-direction, L_x, is assumed to satisfy the condition $a \ll L_x$. The requirements in Eqs. (5) and (6) are rather tough for numerical calculations and thus we relaxed some of these conditions in the calculations.

To be precise, we discuss here how the requirements are alleviated in the FEM calculation. The conditions $d_s \ll d_h \approx d$ are reasonably well-satisfied and the conditions $d \ll L, a$ are well-satisfied, since $d_h = 10 d_s$ (and thus $d = 11 d_s$), $a \approx 500 d_s$ (see below) and $L = 5000\, d_s$ (the condition $a \ll L_x$ is reasonably well satisfied because $L_x = L = 5000 d_s$). While we below compare the three cases in which ε are $\varepsilon_0 = 1/6500, 6.5\varepsilon_0 = 1/1000$, and $65\varepsilon_0 = 1/100$, the condition $\varepsilon^{1/2} L \ll a \approx 500 d_s$ is well satisfied for $\varepsilon = \varepsilon_0$ or 6.5 ε_0. However, this condition is only marginally satisfied (or even moderately violated) for $\varepsilon = 65\ \varepsilon_0$ (although the condition $\varepsilon \ll 1$ is well-satisfied for the three cases) because $\varepsilon^{1/2} L$ is $5000 d_s/10 = 500 d_s$ (that is comparable to a) for $\varepsilon = 65\ \varepsilon_0$. In addition, we should care about the condition $d_h \ll r \ll a$: the scaling regime in a plot as a function of r/d_s (Figure 2) is expected only when $10 \ll r/d_s \ll 500$ even if the other conditions are perfectly satisfied. In addition, the scaling regime in plots as a function of $|r|/(\varepsilon^{1/2} L)$ (Figure 2) can be expected only when $|r| \ll (\varepsilon^{1/2} L)$ in the continuum limit, i.e. if the curve is continuous.

In summary, we have to care about the conditions $d_h \ll r \ll a$ while we should note that the condition $\varepsilon^{1/2} L \ll a$ is only marginally satisfied for $\varepsilon = 65\ \varepsilon_0$; the scaling regimes in graphs whose horizontal axis is r/d_s can be rather narrow and can be expected only for $\varepsilon = \varepsilon_0$ and 6.5 ε_0. In addition, a graph is well explained by the theory only when it suggests a continuum curve when averaged.

2.3. Robustness of the Scating Laws

The scaling laws in Eqs. (2) and (3) state that the stress concentration around the crack tip is reduced by a small factor $\varepsilon^{1/4}$ compared with a monolithic counterpart (hard homogeneous material with elastic modulus E_h) and that the deformation is enhanced around the tip by a large factor $\varepsilon^{-1/4}$. This agree with the results of the numerical calculations at least on a qualitative level, as seen in Figure 2a and d.

2.3.1. Robust Scaling for the Deformation

To see an agreement on a quantitative level, we need to compare the zigzag curves with the smooth curves predicted by the continuum theory. For this purpose, we define average points on the zigzag curves, first for the deformation field: we place the average points at $|r| = nd$ with n integer whose heights are calculated as the weighted average of u_y/u_0 in the range from $|r| = (n-1)d$ to $|r| = (n+1)d$. These points are shown by the three different symbols for $\varepsilon = \varepsilon_0$, 6.5 ε_0, and 65 ε_0. In Figure 2b, we rescale the $|r|$ and u_y axes by $\varepsilon_{1/2} L$ and u_0 according to the predicted scaling law in Eq. (2). As a result, all the average points are collapsed on to a single master curve. This collapse is remarkably well especially if we remind that the conditions for the scaling law in Eqs. (5) and (6) are relaxed so that, at least theoretically, the scaling regimes can be rather narrow and can be expected only for $\varepsilon = \varepsilon_0$ or 6.5 ε_0. This collapse clearly confirms the scaling law in the present numerical model in a robust way. In Figure 2c, the collapse is shown on the log scales. This confirms that the slope is the predicted value 1/2. In addition, the curve starts to deviate from the slope 1/2 when it approaches $r = \varepsilon^{1/2} L$. This is fully consistent with the prediction: this scaling law is valid only under the condition $r \ll \varepsilon^{1/2} L$. The reference line of slope 1/2 in Figure 2c is $y = 5.25 x^{1/2}$ and the line of the same slope that fits the average points in Figure 2c is $y = 1.7 x^{1/2}$ (the latter line is not shown in the figure). This confirms that the numerical coefficient in Eq. (2) is of the order of one, as predicted.

Considering that one of our main scopes of this paper is to show the robustness of the previously proposed scaling laws and we relaxed the sever conditions for the scaling laws, probably we should be satisfied only if the numerical

coefficients corresponding to c_1 and c_2 in front of the scaling laws are confirmed to be of the order of one. However, here we notice that the coefficient 1.7 obtained from Figure 2c is significantly close to the previous prediction $c_1 = 1.6$. Considering the limitations of the FEM calculations this is rather remarkable and may suggest the robustness of the scaling law.

2.3.2. Robust Scaling for the Stress

We next consider a similar averaging for the stress field: we placed average points on the zigzag curves such that the points are placed at $|r| = (n + 1/2)d$ whose heights are calculated as the weighted average of σ_y/σ_0 in the range from $|r| = (n - 1/2)d$ to $|r| = (n + 1/2)d$. The slight difference in the definitions of the average points for deformation and stress comes from technical convenience (remind that the stress is practically constant in each element while the deformation is assigned at boundaries between the elements). In Figure 2e and f, the predicted scaling law in Eq. (3) for $r \ll \varepsilon^{1/2}L$ is clearly confirmed in this numerical model (the reference line of slope $-1/2$ in Figure 2f is $y = 0.24x^{-1/2}$ and the line of the same slope that fits the average points in Figure 2f is $y = 0.55x^{-1/2}$ (not shown in the figure).

Here, if we again dare to discuss the numerical coefficients for the scaling laws, we notice that the latter value of the coefficient 0.55 is reasonably close to the previous prediction $c_2 = 0.4$. The agreement is not so good as in the case of the deformation field. This may be because the stress distribution is singular so that the continuum description is more difficult. Considering this, the agreement for the stress field is still surprising. This again suggests the robustness of the scaling law.

2.3.3. Scaling Law for the Cutoff Stress

As seen in Figure 2d, the tip stress is finite. As mentioned above, this is expected from the original idea in ref.[23,14] In addition, the authors of ref.[23,14] conjectured that this maximum stress should be governed by the scaling law in eq. (4). This conjecture is well confirmed in Figure 3a where the maximum stress at $r = d_s/2$ is plotted as a function of the inverse of the layer thickness d in the renormalized scales defined by Eq. (4) (the slight deviation of the third point from the reference line may be because the condition $\varepsilon^{1/2}L \ll a$ required for the scaling law is well satisfied for the first two points but barely satisfied for the third). The reference line of slope 1/2 in Figure 3a is $y = 1.12x^{1/2}$, which confirms that the numerical coefficient in Eq. (4) is of the order of one (for this coefficient no theoretical prediction exists; even theoretically, it is only known to be of the order of one). In fact, Eq. (4) is also confirmed in Figure 2f by the fact that all the three leftmost points of the three curves where $r = d_s/2$ are almost exactly on the reference line with the slope $-1/2$. This is because this fact directly establishes the relation $\sigma_M/\sigma_0 \simeq \sqrt{\varepsilon^{1/2}L/d_s}$ while $\sqrt{d_s}$ and $\sqrt{d}$ are practically of the same order. Similarly, in Figure 2c, all

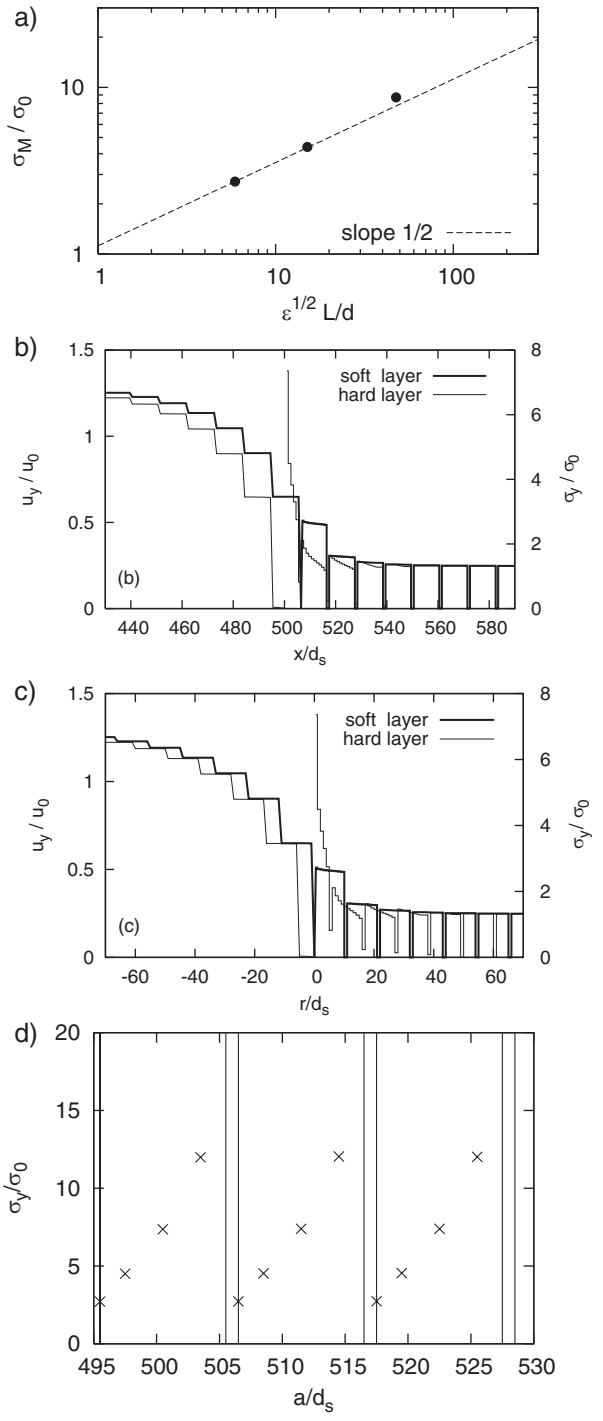

Fig. 3. (a) The maximum stress at a crack tip as a function of the inverse of the layer period d (or cut-off scale) in renormalized log scales. (b) Comparison of the deformation and stress fields as a function of x whose origin is set to the center of cracks, when a crack tip is located at a soft layer and when it is located in the middle of a hard layer. (c) The same comparison as a function of distance r from the crack tips. (d) Stress at the crack tip as a function of crack size. Vertical lines suggest the soft-hard interfaces.

the three rightmost points of the three curves where $|r| = d_s$ are on the reference line with slope 1/2. This suggests a natural prediction from Eq. (2) with the cutoff: the minimum nonzero deformation is determined by the scaling law $u_y/u_0 \simeq \sqrt{|d|/(\varepsilon^{1/2}L)}$. This and Eq. (4) state that the scaling

ADVANCED ENGINEERING MATERIALS

laws in Eqs. (2) and (3) are cut-off at the length scale d of the layered structure.

2.4. Importance of the Crack-Tip Position

2.4.1. Stress and Deformation Near a Crack Tip

Motivated by the original idea in ref.[14,23], up to now we only discuss the case in which the crack tip is located at a soft layer. In contrast, in Figure 3b we compared the deformation and stress fields near the right crack tip when the tip is in the soft layer ($a = 506.5d_s$) and when it is in the hard layer ($a = 500.5d_s$), for $\varepsilon = \varepsilon_0$ as a function of x whose origin is located at the crack center. When we replot the graph as a function of the distance r from the crack tip as in Figure 3c ($r = 0$ corresponds to the right crack tip), we see that the fields for the two crack sizes are similar on the average. However, there are significant differences in the two cases. When the tip is in a hard layer, the deformation in the range from $|r| = 0$ to $|r| = d_h/2$ is severely restricted until it jumps at the first soft layer, and the crack-tip stress (at $r = d_s/2$) is significantly increased.

2.4.2. Mechanism of the Crack Arrest

In Figure 3d, the stress near the tip (at $r = d_s/2$) is plotted as a function of the position of the crack tip. The tip stress tends to increase when the tip moves into a hard layer till the stress is significantly reduced when the tip meets the next soft layer. In other words, the reduction of the stress concentration and the cut-off of the weakly concentrated stress are less effective when a crack tip is located in a hard layer (we confirmed that the scaling law in Eq. (4) is well satisfied even for $a = 500.5d_s$, i.e. when the tip is in a hard layer). This increase of the tip stress as the tip proceeds in a hard layer which is terminated at the soft layer with a significant drop of the stress means that once the crack tip enters a hard layer the tip cannot stop until it meets the soft layer. Namely, the crack tip can stop only in soft layers. This is a clear and explicit demonstration of crack-arrest mechanism that has been discussed for a long time in various contexts.

In addition, in Figure 3d we see that the tip stress as a function of the crack tip position is nearly periodic: the tip stress seems virtually constant irrespective of the crack length. This agrees with the prediction of the scaling law, but confirmed for the first time numerically.

Looking back Figure 1b, we see that, thanks to the large deformation of the soft layers near the tip, the stress is almost completely relaxed with in a few period (d) almost irrespective of the crack length. As a result, the stress distribution around the tip becomes virtually independent of the crack length.

The mechanism of arrest of the crack at a soft layer makes plausible to set a failure condition when crack tips are stopped at a soft layer. In fact, in ref.[14,23], they determined the fracture energy by matching the maximum stress in Eq. (4), which is valid when the tip is arrested at a soft layer as seen above, with the strength of the hard layers, i.e. the failure stress in the Griffith model for Griffith flaws of size a_0: $\sigma_f = \sqrt{E_h\gamma_h/a_0}$. Here, γ_h is the fracture energy per unit area of the hard material.[24] From this matching condition, we obtain the failure stress $\sigma_F \simeq \lambda_\sigma\sqrt{E_h\gamma_h/L}$ for the composite with the enhancement factor $\lambda_\sigma \simeq \varepsilon^{-1/4}\sqrt{d/a_0}$ ($\gg 1$). This failure stress, together with the the Griffith energy balance $(\sigma_F^2/E_h)L \simeq G_c$ where G_c is the fracture energy for the composite, leads to the fracture energy $G_c \simeq \lambda\gamma_h$ with the enhancement factor $\lambda \simeq \varepsilon^{-1/2}(d/a_0)$ ($\gg 1$) and the order of G_c thus obtained matches with the order of an experimentally reported value in the pioneering paper.[2]

3. Conclusions

In this study, we constructed a FEM model for nacre by explicitly taking the layered structure into account. In a previous study, by a bold homogenization, this model reduces to a simple analytical model, which predicts scaling laws for the stress and deformation around a crack tip. In the present study, the numerical simulation is associated with a number of length scales, while only in the limit in which the length scales are well separated with each other the scaling laws are shown to be valid. Although we explicitly include the layered structure and relaxed some of such conditions for calculational convenience, we surprisingly find the same scaling laws for the elastic fields in a clear manner, which establishes the robustness of the scaling laws: the previously predicted scaling law can hold well even when the required conditions are only marginally satisfied. We further found that the scaling laws for the singularity of the stress field near the crack tip is cut-off at the scale of the layer period. In addition, we found that when the crack tip moves into a hard layer the tip stress increases, which forces the arrest of the crack tip at a soft layer. Accordingly, simple physical principles have been established at a quantitative level: nacre is strong and tough because (1) the stress concentration at crack tips is reduced, which is aided by the enhanced deformation near the tips, in such a way that the stress distribution around the tip becomes virtually independent of the crack length. (2) the tip singularity is cut-off at the length of the layer period, and (3) these two effects are made efficient by virtue of the arrest of a crack tip at a soft layer. These mechanisms will be useful as guiding principles for developing reinforced materials. Moreover, the present FEM model will provide a solid basis, at a quantitative level, for studying the toughness of nacre and for developing a new mechanically superior material that mimics nacre.

Received: February 24, 2013
Final Version: March 13, 2013
Published online: May 22, 2013

[1] J. Currey, *Proc. Royal Soc. (London) B* **1977**, *196*, 443.
[2] A. Jackson, J. Vincent, R. Turner, *Proc. Royal Soc. (London) B* **1988**, *234*, 415.
[3] M. Sarikaya, J. Liu, I. Aksay, *Biomimetics: Design and Processing of Materials*, AIP, New York **1995**, p. 35.

[4] B. Smith, T. Schäffer, M. Viani, J. Thompson, N. Frederick, J. Kindt, A. Belcher, G. Stucky, D. Morse, P. Hansma, *Nature* **1999**, *399*, 761.
[5] A. Evans, Z. Suo, R. Wang, I. Aksay, M. He, J. Hutchinson, *J. Mater. Res* **2001**, *16*, 2476.
[6] F. Song, A. Soh, Y. Bai, *Biomaterials* **2003**, *24*, 3623.
[7] D. Katti, K. Katti, J. Sopp, M. Sarikaya, *Comp. Theor. Polymer Sci.* **2001**, *11*, 397.
[8] P. Nukala, S. Zapperi, S. Šimunović, *Phys. Rev. E* **2005**, *71*, 066106.
[9] T. Kato, *J. Adv. Mater.* **2000**, *12*, 1543.
[10] M. Sarikaya, C. Tamerler, A. Jen, K. Schulten, F. Baneyx, *Nat. Mater.* **2003**, *2*, 577.
[11] E. Munch, M. Launey, D. Alsem, E. Saiz, A. Tomsia, R. Ritchie, *Science* **2008**, *322*, 1516.
[12] L. Bonderer, A. Studart, L. Gauckler, *Science* **2008**, *319*, 1069.
[13] L. Corte, L. Leibler, *Macromolecules* **2007**, *40*, 5606.
[14] K. Okumura, P.-G. de Gennes, *Eur. Phys. J. E* **2001**, *4*, 121.
[15] Y. Aoyanagi, K. Okumura, *Phys. Rev. Lett.* **2010**, *104*, 038102.
[16] P. Ball, *Nat. Mater.* **2010**, *9*, 190.
[17] S. Cranford, A. Tarakanova, N. Pugno, M. Buehler, *Nature* **2012**, *482*, 72.
[18] X. Li, W. Chang, Y. Chao, R. Wang, M. Chang, *Nano Lett.* **2004**, *4*, 613.
[19] F. Barthelat, C. Li, C. Comi, H. Espinosa, *J. Mater. Res.* **2006**, *21*, 1977.
[20] Y. Hamamoto, K. Okumura, *Phys. Rev. E* **2008**, *78*, 026118.
[21] Y. Aoyanagi, K. Okumura, *Phys. Rev. E* **2009**, *79*, 066108.
[22] T. Sumitomo, H. Kakisawa, Y. Owaki, Y. Kagawa, *J. Mater. Res.* **2008**, *23*, 1466.
[23] P.-G. de Gennes, K. Okumura, *Comp. Ren. Acad. Sci. IV* **2000**, *1*, 257.
[24] B. Lawn, *Fracture of Brittle Solids*, 2nd edition, Cambridge Univ. Press, Cambridge **1998**.

